Strain in lattice mismatched CdSe-based core/shell nanoplatelets

Jordi Llusar, Josep Planelles, and Juan I. Climente*

Departament de Química Física i Analítica, Universitat Jaume I, E-12080, Castelló de la Plana, Spain

E-mail: climente@uji.es

Abstract

We investigate the role of the stress arising between core and shell materials in colloidal CdSe/X hetero-nanoplatelets (X=ZnS,CdS,CdTe). The resulting strain distribution is calculated within the linear elastic regime, and its influence on the electronic structure with k·p theory. We show that strain shifts the energy of electrons and that of holes by several tens of meV. In structures with type-I band alignment the two shifts have opposite signs and the net effect on the exciton emission energy is small, but in type-II systems they add up. The strain response in colloidal NPLs is found to exhibit some differences as compared to that of epitaxial quantum wells, including sizable influence of lateral dimensions below 10 nm and potentially relevant effect of coupled strain-momentum terms of the Hamiltonian. We further show that asymmetric shell covering leads to bending of the nanoplatelet and tilted potential profiles along the strong confinement direction, analogous to a built-in electric field. We propose overcoating CdSe/CdS NPLs with an outer ZnS shell as a method to mitigate tunneling-induced redshift of emission via strain engineering.

Introduction

In the last decade, quasi-two-dimensional colloidal metal chalcogenide semiconductors –often referred to as nanoplatelets (NPLs)– have emerged as an alternative to quantum dots for a variety of optoelectronic applications.[1] Many properties of interest have been reported, often related to their 2D dimensionality. Thus, precisely controllable quantum confinement in one direction enables narrow emission linewidths and reduced Auger recombination rates. At the same time, the large in-plane area grants large absorption cross-sections and giant oscillator strength through exciton correlation.[1–4]

The large surface-to-volume ratio of NPLs makes them highly sensitive to the environment.[5,6] Attempts have been made to passivate the surface of CdSe NPLs by growing either core/crown heterostructures[7,8] or core/shell ones,[9–12,15] which have succeeded in improving the emission quantum yield and stability. However, the addition of shell materials has a profound impact on the electronic structure too. As compared to core-only CdSe NPLs, CdSe/ZnS hetero-NPLs display redshifts of up to 300-400 meV and CdSe/CdS ones up to 500 meV.[12–14,16,17] The origin of such a large redshift has been discussed in the literature. Some studies suggest it simply arises from carrier tunneling into the shell, which relaxes quantum confinement.[13,14,17] Others claim instead that tunneling in CdSe/ZnS is hindered by the large band-offset (around 1 eV) and suggest the decrease in dielectric confinement upon shell growth provides an additional, non-negligible contribution to the redshift.[12] On the other hand, CdSe has significant lattice mismatch with both CdS (4%) and ZnS (12%). Therefore, strain is also expected to play a role. Achtstein et al. calculated the effect of linear elastic strain on the exciton energy of CdSe/CdS NPLs, and concluded it gives a moderate blueshift of the exciton energy.[17] By contrast, Luo et al. grew CdSe/ZnS NPLs for solar cell devices and inferred from photoluminescence and open current voltage measurements that strain was producing a redshift, and possibly type-II band alignment.[18] In this context, a thorough study of the influence of elastic strain in lattice mismatched hetero-NPLs is on demand.

In free-standing colloidal hetero-nanocrystals, strain engineering has proved to be a powerful tool to modulate exciton energy and wave function, with direct implications on the optoelectronic response.[19–21] Likewise, in epitaxial quantum wells, strain engineering of the band structure has been key to reducing lasing threshold and optimizing laser performance.[22] Since core/shell NPLs are the colloidal analogous of epitaxial quantum wells, the question arises of whether strain can also give rise to significant changes of the electronic structure, and whether they take place in the same way as in epitaxial quantum wells. In this work, we address such questions for lattice mismatched hetero-NPLs.

We study core/shell NPLs with binary CdSe/X composition (X=CdS, ZnS, CdTe). The strain is calculated within linear elastic theory, and the effect of the resulting deformation potential on excitons is computed with effective mass Hamiltonians fully including electronic correlation effects, which are critical in these structures owing to the weak lateral spatial confinement and strong dielectric mismatch.[26,27] We find that the strain response of colloidal NPLs is reminiscent of that epitaxial quantum wells, albeit with some qualitative differences. The finite lateral size of the NPL influences the strain value in the core for dimensions below $\sim$ 10 nm. Also, coupled strain-momentum terms of the Hamiltonian, which are negligible in epitaxial systems, have a moderate impact on the exciton energy (up to tens of meV) due to the stronger quantum confinement of colloidal structures. In CdSe/CdS and CdSe/ZnS NPLs, the compressive strain inside the core blueshifts and redshifts electron and hole energies, respectively. For neutral excitons, the two effects tend to compensate and the energetic imprint of strain is weak. The effect is stronger for excitons in type-II CdSe/CdTe NPLs, as the electron stays in the tensiled core but the hole migrates into the compressed shell, so that the two carriers redshift. In all cases, however, the strain effect on the emission energy is found to be secondary as compared to tunneling into the shell. We propose the use of ternary structures, such CdSe/CdS/ZnS NPLs, as a means of decoupling tunneling and strain effects. Interestingly, we show that a slightly asymmetric shell covering –different number of shell monolayers (MLs) on top and bottom sides of the core– can explain the

bending of NPLs observed in recent experiments with CdSe/ZnS NPLs.[12]

Methods

Strain maps are calculated by minimizing the elastic energy in the anisotropic continuous mechanical model.[28] The boundary conditions are zero normal stress for the free surface.[29] The strain tensor elements $\epsilon_{ij}(\mathbf{r})$ is obtained using the multiphysics mode of Comsol 4.2 software. Exciton states are calculated following Ref.,[26] but adding strain-induced potential terms. Thus, excitons are described by the Hamiltonian:

$$H^X = H^e + H^h + V^{e-h} + E_\Gamma^{gap}, \tag{1}$$

where E_Γ^{gap} is the bulk band gap of CdSe at the Γ point, V^{e-h} is the electron-hole Coulomb attraction including dielectric mismatch enhancement, and H^j are the single-particle Hamiltonians for electron ($j = e$) and hole ($j = h$). These are 3D single-band k·p Hamiltonians of the form $H^j = H^j_{kin} + V^j$, where H^j_{kin} is the kinetic energy term and V^j the single-particle potential. The latter can be split into several terms:

$$V^j = V^j_{bo} + V^j_{self} + V^j_{strain}. \tag{2}$$

where V^j_{bo} is the spatial confining potential defined by the (bulk) band offsets between CdSe and the shell material, V^j_{self} the self-interaction potential due to the inhomogeneous dielectric environment, and V^j_{strain} the strain-induced potential. Within deformation potential theory, up to first order in ϵ and second in k, the general form of the strain terms in a k·p Hamiltonian is :[22]

$$H_{strain} = \mathbf{D}^{\boldsymbol{\varepsilon}} \cdot \boldsymbol{\varepsilon} - \frac{\mathbf{k}\boldsymbol{\varepsilon}\mathbf{k}}{m_0} - 2\,\frac{\boldsymbol{k}\boldsymbol{\varepsilon}\boldsymbol{p}}{m_0}. \tag{3}$$

Here, $\boldsymbol{\varepsilon}$ and $\mathbf{D}^{\boldsymbol{\varepsilon}}$ the strain and deformation potential tensors, m_0 the free electron mass, $\boldsymbol{k}$ the momentum operator acting on the envelope function and $\boldsymbol{p}$ that acting on the (microscopic)

Bloch function. The second term in Eq. (3) describes the change in the kinetic energy due to the strain, and it is generally neglected in the study of epitaxial quantum wells because it is expected to be smaller than terms containing ε alone.[22] However, we keep the k_z component because the strong confinement of colloidal NPLs along [001] suggests it can become relevant, as we confirm in the next section. When projected on the conduction band (CB) Bloch function, Eq. (3) gives rise to $V^e_{strain} = V^{dp,e}_{strain} + V^{pz,e}_{strain}$, with:

$$V^{dp,e}_{strain} = a_c \left(\varepsilon_{xx} + \varepsilon_{yy} + \varepsilon_{zz}\right), \tag{4}$$

and

$$V^{pz,e}_{strain} = -\frac{k_z \epsilon_{zz} k_z}{m^*_{e,z}}, \tag{5}$$

Here a_c is a material dependent deformation potential coefficient, $k_z = -i\hbar\, d/dz$ and $m^*_{e,z}$ the electron effective mass along z. Notice the last term of Eq. (3) vanishes in V^e_{strain} because $\boldsymbol{p}$ has odd parity. Likewise, when projected on the valence band (VB) heavy hole Bloch function, Eq. (3) gives $V^h_{strain} = V^{dp,h}_{strain} + V^{pz,h}_{strain}$, with:

$$V^{dp,h}_{strain} = \left(a_v + \frac{b}{2}\right)\left(\varepsilon_{xx} + \varepsilon_{yy}\right) + (a_v - b)\varepsilon_{zz}, \tag{6}$$

and

$$V^{pz,h}_{strain} = -\frac{k_z \epsilon_{zz} k_z}{m^*_{h,z}}, \tag{7}$$

where a_v and b are deformation potential coefficients, and $m^*_{h,z}$ the hole effective mass along z. As we shall see below, strain is roughly constant around the center of the NPL plane, where most of the charge density is located. For this reason, it is a good approximation to describe V^e_{strain} and V^h_{strain} simply as functions of z, taken along the axis orthogonal to the NPL plane. Piezoelectric terms are neglected in this study because they are negligible in CdSe-based hetero-NPLs with cubic crystal structure.[17]

Hamiltonian (1) is solved variationally by optimizing the effective exciton Bohr radius.[26]

Material parameters used in the calculation are given in the Supporting Information.

Results and discussion

Our goal is to study the strain distribution in core/shell NPLs and its influence on the electronic structure. We first analyze in detail the prototypical case of CdSe core surrounded by a shell of CdS, ZnS or CdTe. The shell is symmetric on top and bottom. Next, we analyze the effect of having asymmetric shell coating, and show that this deviation from ideality can explain a few features observed in recent experiments. Last, building on the behavior observed in previous sections, we briefly address the case of ternary NPLs, to illustrate the potential of strain engineering in such systems.

Symmetric core/shell NPLs

Finite and controllable lateral confinement is a distinct feature of colloidal NPLs as compared to epitaxial quantum wells. We then start by studing if it has a significant effect on the strain experienced inside the platelet. We consider CdSe/CdS NPLs with 4.5 ML CdSe core and 5 ML shell thickness, and calculate the hydrostatic strain, $\varepsilon_{hyd} = \varepsilon_{xx} + \varepsilon_{yy} + \varepsilon_{zz}$, for the three different lateral dimensions shown in Figure 1(a-c).

In general, ε_{hyd} is compressive in the CdSe core and tensile in the CdS shell (Fig. S1). Because the ground state charge density is mostly localized inside the core, it is worth inspecting this region in detail. The corresponding values of ε_{hyd} on the mid-height xy plane of the core are plotted in Figure 1(d-f), and a cross-section comparing the strain in all three structures along the x semi-axis is shown in Figure 1(g). The general behavior is as follows. A flat area of compressive strain ($\varepsilon_{hyd} < 0$) is formed around the center of the NPL, which extends towards the sides. About 5 nm before reaching the border, the strain becomes slightly more compressive and in the close vicinity of the border (< 1 nm), it switches to tensile ($\varepsilon_{hyd} > 0$). The compressive character is because of the larger lattice constant of the

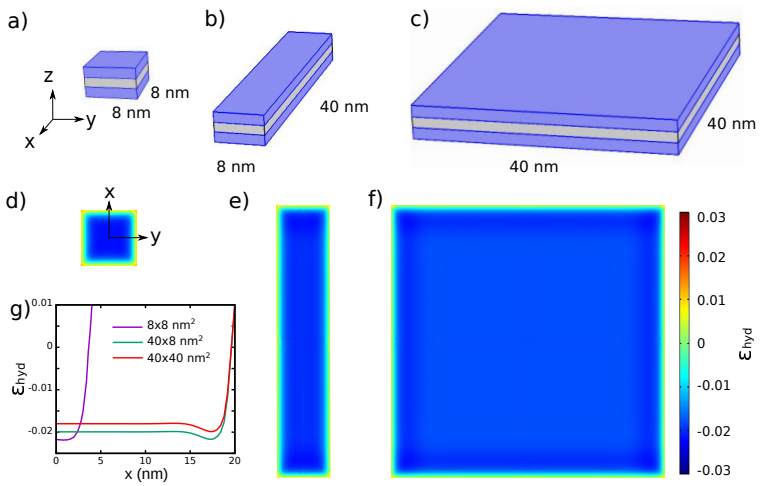

Figure 1: Effect of the lateral sides on strain. (a-c) Schematic of core-shell NPLs with different lateral dimensions. The CdSe core has 4.5 ML and the CdS shell 5 ML thickness. (d-f) Corresponding values of hydrostatic strain over the xy plane at mid-height of the core. (g) Hydrostatic strain cross-section along the x semi-axis for different lateral dimensions. A flat area of compressive strain is formed around the center, with deviations in the vicinity ($\sim$ 5 nm) of the borders. NPLs with smaller lateral dimensions are more compressed.

CdSe core, which needs to shrink to reduce lattice mismatch with the CdS shell. The tensile character near the borders, instead, is a compensation for the central contraction, which is facilitated by the absence of forces acting on the lateral sides.

Since the strain potential felt by electrons is $V^e_{strain} = a_c\,\varepsilon_{hyd}$, with $a_c = -2$ eV for CdSe, the increase in compressive character near the borders gives rise to a small potential barrier, while the sudden switch to tensile strain yields a narrow potential well near the borders. These effects modify the effective size of the NPL because quantum confinement in the plane is very weak, but the ground state wave function is only slightly perturbed and stays around the center of the core (Fig. S2). In the center of the core, strain is also affected by lateral confinement, as ε_{hyd} grows stronger with decreasing dimensions –20% increase from 40×40 nm^2 to 8×8 nm^2, see Fig. 1(g)–. This will blueshift the electron energy through V^e_{strain} by a several meV. It is worth noting that this magnitude is comparable to that of lateral quantum confinement itself,[26,30] and provides a source of linewidth broadening in ensembles of core/shell NPLs.

In what follows, we focus on NPLs with 40×8 nm^2 sides, which is close to the experi-

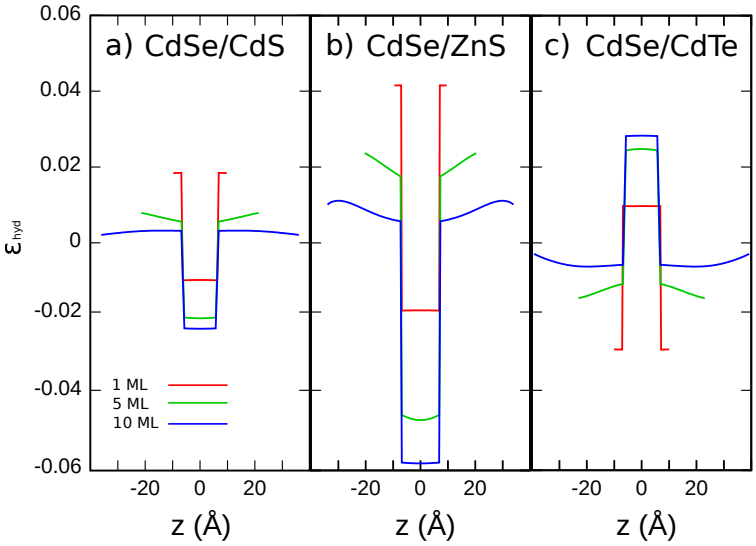

Figure 2: Effect of shell thickness and composition on the hydrostatic strain. (a) CdSe/CdS NPL. (b) CdSe/ZnS NPL. (c) CdSe/CdTe NPL. The strain is taken along the z axis, passing through the NPL center, normal to the its surface.

mental dimensions of recent works.[12,13] In Figure 2 we study the effect of shell thickness and composition on ε_{hyd} along the z axis. For CdSe/CdS and CdSe/ZnS, the strain is compressive in the core and tensile in the shell, while the opposite occurs for CdSe/CdTe because the lattice constant of the CdTe shell is larger than that of the CdSe core. In all cases, the core (shell) becomes more (less) strained with increasing shell thickness. This is because the thicker material forces the thinner one to endure most of the deformation. The net compressive (CdS, ZnS shells) or tensile (CdTe shell) character of ε_{hyd} in the core is given by $\varepsilon_{xx}+\varepsilon_{yy}$. Since the interface between core and shell lies on the xy plane, the magnitude of this term is larger than that of ε_{zz}, which has opposite sign as expected from the Poisson ratio (see Figure S3). This is precisely the opposite behavior to that of core/shell nanorods.[29] In the center of the NPL, we find the ratio between lateral contraction and vertical expansion –or vice-versa– closely follows the biaxial strain expression for cubic crystals, $\varepsilon_{zz} = -2c_{12}/c_{11}\,\varepsilon_{xx}$, as in epitaxial quantum wells.[22]

From the diagonal elements of the strain tensor one can infer the strain-induced deformation potential, $V^{dp,e}_{strain}$ and $V^{dp,h}_{strain}$, which we plot in Figure 3. The figure shows that, inside compressed cores, a shift of the CB bottom to higher energies takes place, which saturates

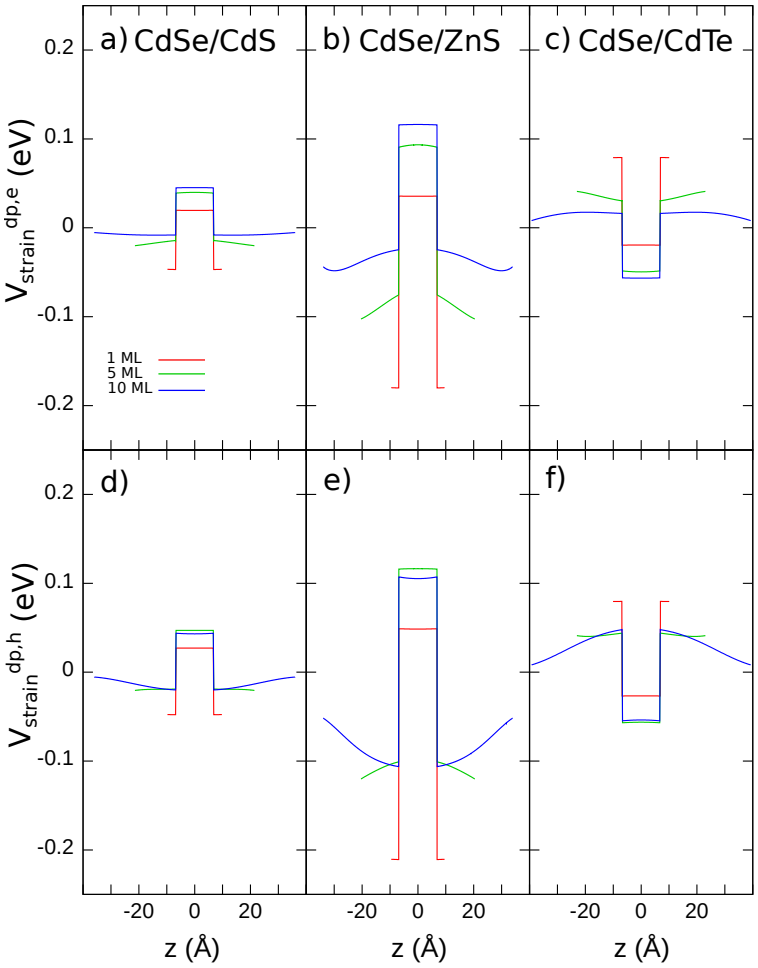

Figure 3: Effect of shell thickness and composition on the deformation potential for CB (top panels) and VB (bottom panels). (a,d) CdSe/CdS NPL. (b,e) CdSe/ZnS NPL. (c,f) CdSe/CdTe NPL.

at about 50 meV (CdSe/CdS, Fig. 3(a)) and 120 meV (CdSe/ZnS, Fig. 3(b)). Conversely, when the core is under tensile strain (CdSe/CdTe), the CB shifts to lower energies (down to -60 meV, Fig. 3(c)). This modifies the band offsets seen by electrons, providing energetic corrections which have been overlooked in previous simulations of hetero-NPLs disregarding strain.[12–14,26] The good agreement between theory and experiments in such works is because for holes the behavior is similar to that of electrons. As shown in Fig. 3(d-f), strain also shifts the VB top towards higher (lower) energies when the core is compressed (expanded).[31] Even the magnitude of the shift is comparable, despite the anisotropic nature of $V_{strain}^{dp,h}$. Then, the shift of electrons and holes partially compensate, and the exciton emission energy is not

expected to change drastically.

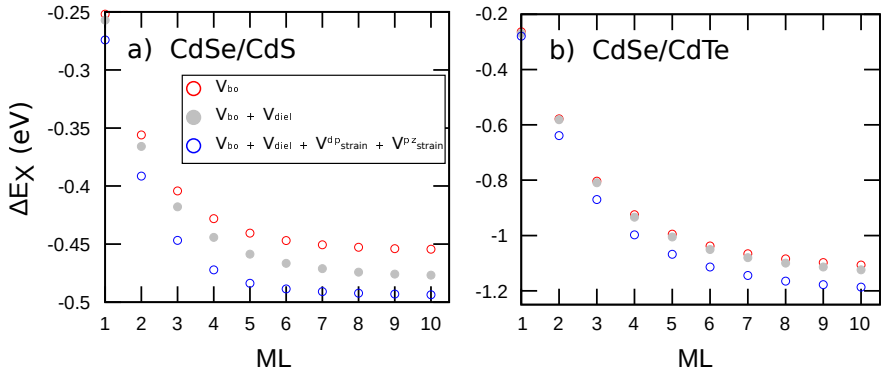

Figure 4: Exciton energy as a function of the shell thickness in (a) CdSe/CdS and (b) CdSe/CdTe NPLs. Red circles show results considering tunneling only. Grey dots include dielectric effects too. Blue circles further add strain effects. All energies are referred to that of the exciton in core-only CdSe NPL.

To better visualize and understand the role of strain on the exciton ground state, we calculate its energy from H^X, with full inclusion of in-plane Coulomb interaction, for different shell natures. First, we focus on the case of CdSe/CdS NPLs. Fig. 4(a) shows the exciton energy shift in CdSe NPLs with n MLs of CdS shell on each side, as compared to the core-only CdSe NPL. Red circles show the case where dielectric confinement (V^j_{self}, polarization of V^{e-h}) and strain terms (V^j_{strain}) are neglected. The exciton is then found to redshift by 454 meV upon shell growth, due to electron leaking into CdS. The inclusion of dielectric confinement terms gives rise to an additional redshift of up to 23 meV (grey dots). This effect was noticed in Ref.[12] and is a consequence of the suppression of self-interaction potential energy. Further including strain terms provides yet an extra 17 meV redshift (blue circles). As anticipated above, the energetic effect of strain is relatively small, owing to the compensation of electron and hole shifts. We note that a previous theoretical study indicated that strain in CdSe/CdS NPLs gives rise to a blueshift instead.[17] This is due to the different parameters used for deformation potential and elastic constants, as there is enough dispersion in the literature to change the net sign of strain energy perturbation (see discussion in SI). In any case, for all set of parameters we find that in CdSe/CdS NPLs strain is secondary term (few tens of meV) as compared to tunneling (hundreds of meV).

Next we consider the case of CdSe/CdTe NPLs. As can be seen in Fig. 4(b) –cf. blue circles and grey dots–, here strain produces an exciton energy redshift up to 63 meV, almost 4 times larger than in CdSe/CdS. This is because of the type-II band alignment, which places the electron inside the tensiled CdSe core and the hole inside the compressed CdTe shell. Then, both carriers redshift and there is no cancellation. However, the strain effect is still but a perturbation to the confinement energy set by the staggered band-offset (red dots in the figure).

In CdSe/ZnS NPLs, photoluminescence experiments have shown shell growth leads to a large redshift (300-400 meV, for 4.5 ML cores).[12,14] Because the band-offset between CdSe and ZnS is around 1 eV, tunneling is expected to be less important than with CdS or CdTe shells. By contrast, the lattice mismatch is large (over 10%). For this reason, some studies have suggested strain may play a chief role in determining the redshift, and may even lead to a type-II band alignment.[18] To clarify the influence of strain in these structures, in Figure 5 we plot the exciton energy as a function of the ZnS shell thickness. The result is similar to that of CdSe/CdS, with a large redshift whose main contribution (320 meV) comes from tunneling. Strain provides a redshift of about 34 meV, which is 1.5 times larger than the dielectric confinement suppression proposed in Ref.[12] All in all, the redshift is mostly due to tunneling plus strain, with no need to invoke indirect excitons, as the band alignment stays type-I –see Fig. 3–. Further, we note that strain builds up gradually with increasing shell thickness. Consequently, in Fig. 5 the energy splitting between strained (blue circles) and unstrained (red circles) exciton shifts increases from 1 to 5 ML. Therefore, the large redshift (up to 200 meV) reported by photoluminescence and atomistic studies upon growth of the first ML of shell[16,17,32,33] must be associated primarily with the reduced spatial confinement, with a minor contribution from strain.

The blue circles in Figure 5 indicate that the fully strained exciton should have minimum energy between 4-5 MLs of ZnS. The origin of this inflection point is as follows. With increasing strain, the electron energy blueshifts and that of the hole redshifts, due to changes

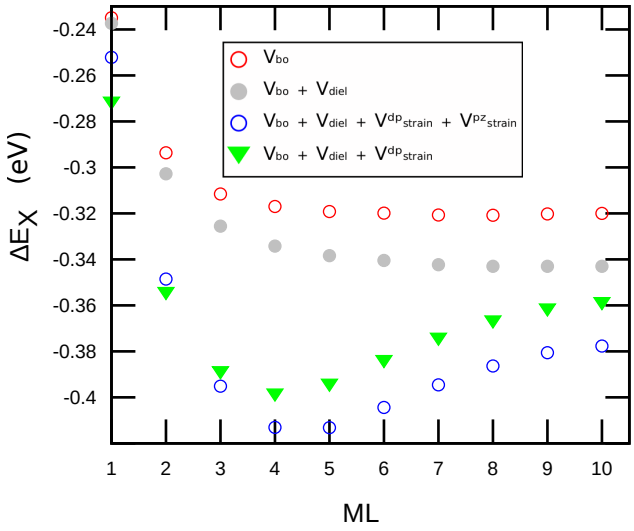

Figure 5: Exciton energy as a function of the shell thickness in CdSe/ZnS. Energies are referred to that of the exciton in core-only CdSe NPL. Strain has a stronger contribution to the overall redshift than in CdSe/CdS. A sizable part of the redshift is due to the relaxed quantum confinement when the CdSe core expands vertically, $V_{pz,e} + V_{pz,h}$. V_{diel} stands for dielectric effects (V_{self} and polarization of V^{e-h}).

in the deformation potential reported in Fig. 3(b) and (e). For 1-5 ML, the hole redshift dominates over the electron blueshift. With increasing shell thickness, however, vertical expansion of the core becomes more difficult. Then, ε_{zz} saturates around 4-5 ML. Since the hole redshift is mostly given by $(a_v - b)\,\varepsilon_{zz}$, from this distance on the electron blueshift takes over. We have tested that the minimum is robust to different sets of material parameters and interface alloying effects. However, it has not been observed in available experiments so far, where exciton emission energy decreases monotonically.[12,14] A possible interpretation of the experimental results is given in the next section.

To close the study of symmetric core/shell NPLs, we note that a recent study about the influence of surface ligands on CdSe NPL emission has suggested that the strain induced by ligands is responsible for large exciton redshifts of up to 250 meV.[23] The underlying idea is that the compressive in-plane stress gives rise to transversal expansion, which in turn reduces the extreme quantum confinement. While our continuum mechanical model is not suitable for the study of molecular ligands, we investigate if a similar effect can be expected in strained core/shell structures. The reduced quantum confinement due to transversal

expansion should be captured by coupled momentum-strain operators, $V^{pz,e}_{strain}$ and $V^{pz,h}_{strain}$ in Eqs. (5) and (7). Green triangles in Fig. 5 show the energy of strained excitons neglecting V^{pz}_{strain} terms, while blue circles show the fully strained system. The comparison reveals that the strain-induced expansion of the core gives rise to a redshift of about 20 meV, comparable to the contribution of deformation potential terms, V^{dp}_{strain}. This is one order of magnitude smaller than the redshift suggested for ligand-induced strain,[23] but clearly larger than in epitaxial quantum wells, where these terms are systematically neglected arguing they are much weaker than (linear-in-ε) deformation potential terms. The different behavior arises from quantum confinement in colloidal NPLs being much stronger than in epitaxial wells, with higher potential barriers –set by the ligands– and often thinner dimensions.[3,24]

Asymmetric core/shell NPLs

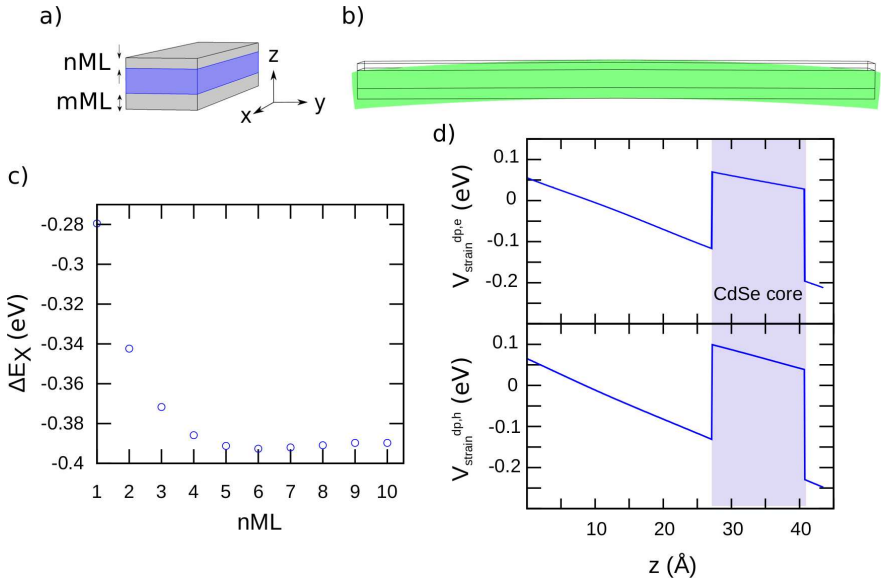

Figure 6: CdSe/ZnS NPLs with asymmetric shell distribution. (a) Schematic of the structure. Different number of shell MLs n and m are considered. (b) Total displacement of the NPL upon strain relaxation in a NPL with $n = 5$ and $m = 6$. Notice the bending on the sides. (c) Exciton energy shift as a function of shell thickness. $m = n + 1$. The energy decreases monotonically and stabilizes around 5 MLs, in agreement with experiments. (d) Deformation potential for electrons and holes in a NPLs with $n = 1$ and $m = 10$. The asymmetric shell gives rise to a small tilting of the potential.

The growth of shells around a core NPL is susceptible of small accidental or intentional asymmetries. We then consider a CdSe/ZnS NPL with n and m ZnS MLs on the top and bottom sides of the core, respectively –see schematic in Fig. 6(a)–. Interestingly, in such a structure a single ML difference between n and m suffices to give rise to bent hetero-NPLs, owing to the unbalanced strain on top and bottom sides. An example is plotted in Fig. 6(b). The presence of bending is in fact consistent with high-angle annular dark-field scanning transmission electron microscope images of thick shell CdSe/ZnS NPLs.[12] We have tested that the bending does not modify the electron and hole wave function localization significantly, as they stay near the center. Yet, it has a clear impact on the emission energy. In Fig. 6(c) we plot the exciton shift with respect to the core-only NPL with increasing shell thickness, keeping one extra ML for the bottom shell ($m = n + 1$). Unlike in the symmetric case, the shift now decreases monotonically, in agreement with the experiments in Refs.[12,14] Both the bending and the smooth redshift support the hypothesis that CdSe/ZnS hetero-NPLs may have slightly asymmetric shell. It is worth noting that the asymmetric strain also induces band tilting through V^{dp}_{strain} terms. This is illustrated in Fig. 6(d). In Ref.,[18] CdSe NPLs deposited on a porous TiO_2 film were overcoated with ZnS. This synthetic procedure may lead to severe shell asymmetry. In principle, the asymmetry and the resulting band tilting –which acts as an built-in electric field, and increases with the difference between m and n– may explain the type-II band alignment inferred from the experiments. However, we find that even for large differences between m and n, the field is only of 35 meV/nm. Considering the strong confinement in the z direction, it is not enough to separate electrons from holes.

Core/shell/shell NPLs

As mentioned before, the use of CdS shells to passivate the CdSe NPL surface can improve the emission quantum yields and stability. However, it necessarily implies a redshift of the emission wavelength due to the reduced quantum confinement, dielectric and strain effects

discussed in previous sections. This is sometimes an undesired side effect, as one may want to preserve high emission energy. In this section we propose a means of partially mitigating the redshift, by exploiting the different sensitivity of CB and VB deformation potential to the shell thickness, which we noticed in the analysis of Fig. 5. The idea is to design a ternary NPL, where the CdSe/CdS NPL is overcoated with ZnS, as plotted in Fig. 7(a). Fig. 7(b) shows the exciton energy shift upon ZnS coating. If the thickness of the CdS shell is small (2 MLs, left panel), the effect of ZnS is producing a small additional redshift ($\Delta E_X < 0$), since it facilitates tunneling as compared to organic ligands. However, as CdS grows thicker (5 MLs, right panel), tunneling effects saturate and one observes strain effects only. Then, ZnS starts blueshifting the exciton energy ($\Delta E_X > 0$). For thick ZnS shells, the blueshift can reach around 60 meV. This is in contrast with the behavior of binary (core/shell) CdSe/ZnS NPLs reported in Fig. 5, where the main effect of ZnS is to redshift.

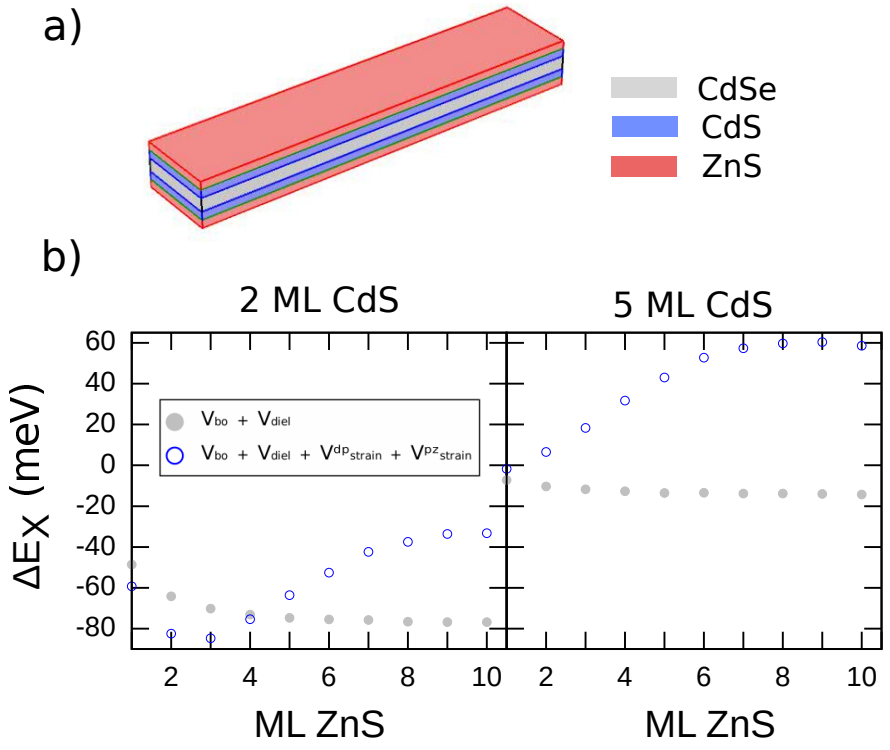

Figure 7: (a) Schematic of the core/shell/shell NPL under study. (b) Exciton energy shift as a function of the number of MLs of ZnS surrounding CdSe/CdS NPL. Left: CdS has 2 ML thickness. Right: CdS has 5 ML thickness. Energies are referred to that of CdSe/CdS NPL. The strain induced by the outer ZnS shell can give rise to a blueshift of tens of meV.

The origin of the strain induced blueshift when adding ZnS is reminiscent of that observed in Fig. 5 beyond 5 MLs. Since ZnS has smaller lattice constant than CdSe and CdS, it further compresses the core in the in-plane direction ($\varepsilon_{xx}+\varepsilon_{yy}$). However, its bonds are stiff, so that vertical expansion ε_{zz} is inhibited with increasing ZnS thickness (see Fig. S4). The compensation between electron blueshift and hole redshift is then quenched, as the latter arises from $(a_v-b)\,\varepsilon_{zz}$, see Eq. (6). The blueshift induced by ZnS in Fig. 7(b) may be underestimated, because the value of a_c we have chosen for CdSe is among the smallest proposed in the literature. Photoluminescence experiments with these structures may provide direct measures of the strain induced blueshift, and prove the operating principle, which can then be transferred to other materials. We stress that observing a blueshift would additionally confirm that core/shell/shell structures enable separate engineering of tunneling and strain effects.

Conclusions

In summary, we have investigated theoretically the role of linear elastic strain in core/shell NPLs based on CdSe. The main findings are: (i) the finite lateral side of NPLs influences the strain value up to 5 nm away from the borders; (ii) coupled strain-momentum terms of the strain Hamiltonian, which are generally neglected in epitaxial quantum wells, can be comparable to deformation potential terms in strongly strained NPLs (e.g. CdSe/ZnS), owing to the stronger quantum confinement of colloidal structures; (iii) the energetic influence of strain is larger in type-II systems (e.g. CdSe/CdTe) than in type-I ones (CdSe/CdS, CdSe/ZnS) because in the latter electrons and holes have opposite response to strain. In any case, the energetic influence reaches several tens of meV at most. This is secondary as compared to tunneling, which remains as the main responsible for exciton redshift even in CdSe/ZnS NPLs. (iv) single-ML asymmetry in the shell growth can explain the NPL bending and smooth exciton energy decay vs. shell thickness in Ref.[12] (v) the use of ternary

(core/shell/shell) NPLs enables separate engineering of tunneling and strain, opening a route to partially compensate for the large redshift obtained when passivating CdSe cores with a single shell.

Acknowledgement

Support from MINECO project CTQ2017-83781-P and UJI project B2017-59 is acknowledged.

Supporting Information Available: Further details of material parameters and additional calculations on the electron and hole wave function in-plane distribution, strain tensor components ($\varepsilon_{xx} + \varepsilon_{yy}$ vs ε_{zz}) in binary (core/shell) and ternary (core/shell/shell) NPLs, as well as ensuing CB and VB potentials.

References

(1) Kovalenko M.; Manna L.; Cabot A.; Hens Z.; Talapin D.V.; Kagan Ch.R.; Klimov V.I.; Rogach A.L.; Reiss P.; Milliron D.J.; *et al.* Prospects of Nanoscience with Nanocrystals. *ACS Nano* **2015**, *9*, 1012-1057.

(2) E. Lhuillier, S. Pedetti, S. Ithurria, B. Nadal, H. Heuclin, B. Dubertret. Two-Dimensional Colloidal Metal Chalcogenides Semiconductors: Synthesis, Spectroscopy, and Applications. *Acc. Chem. Res.* **2015**, *48*, 22 - 30

(3) S. Ithurria, M. D. Tessier, B. Mahler, R. P. S. M. Lobo, B. Dubertret and Al. L. Efros, Colloidal nanoplatelets with two-dimensional electronic structure. *Nature Materials* **2011**, *10*, 936-941.

(4) J. Planelles, A. W. Achtstein, R. Scott, N. Owschimikow, U. Woggon, and J. I. Cli-

mente. Tuning Intraband and Interband Transition Rates via Excitonic Correlation in Low-Dimensional Semiconductors. *ACS Photonics* **2018**, *5 (9)*, 3680-3688

(5) M. Lorenzon, S. Christodoulou, G. Vaccaro, J. Pedrini, F. Meinardi, I. Moreels, and S. Brovelli. Reversed oxygen sensing using colloidal quantum wells towards highly emissive photoresponsive varnishes. *Nature Communications* **2015**, *6*, 6434

(6) S. Singh, R. Tomar, S. ten Brinck, J. de Roo, P. Geiregat, J. C. Martins, I. Infante and Z. Hens. Colloidal CdSe Nanoplatelets, A Model for Surface Chemistry/Optoelectronic Property Relations in Semiconductor Nanocrystals. *J. Am. Chem. Soc.* **2018**, *140*, 13292-13300

(7) A. Prudnikau, A. Chuvilin and M. Artemyev. CdSe–CdS Nanoheteroplatelets with Efficient Photoexcitation of Central CdSe Region through Epitaxially Grown CdS Wings. *J. Am. Chem. Soc.* **2013**, *135*, 14476-14479

(8) M. D. Tessier, P. Spinicelli, D. Dupont, G. Patriarche, S. Ithurria and B. Dubertret. Efficient Exciton Concentrators Built from Colloidal Core/Crown CdSe/CdS Semiconductor Nanoplatelets. *Nano Lett.* **2014**, *14*, 207-213

(9) B. Mahler, B. Nadal, C. Bouet, G. Patriarche and B. Dubertret. Core/Shell Colloidal Semiconductor Nanoplatelets. *J. Am. Chem. Soc.* **2012**, *134*, 18591-18598

(10) M. D. Tessier, B. Mahler, B. Nadal, H. Heuclin, S. Pedetti and B. Dubertret. Spectroscopy of Colloidal Semiconductor Core/Shell Nanoplatelets with High Quantum Yield. *Nano Lett.* **2013**, *13*, 3321-3328

(11) A. A. Rossinelli, A. Riedinger, P. Marqués-Gallego, P. N. Knüsel, F. V. A. and D. J. Norris. *Chem. Commun.* **2017**, *53*, 9938-9941

(12) A. Polovitsyn, Z. Dang, J. L. Movilla, B. Martín-García, A. H. Khan, G. H. V. Bertrand,

R. Brescia and I. Moreels. Synthesis of Air-Stable CdSe/ZnS Core–Shell Nanoplatelets with Tunable Emission Wavelength. *Chem. Mater.* **2017**, *29*, 5671-5680

(13) H. Cruguel, C. Livache, B. Martinez, S. Pedetti, D. Pierucci, E. Izquierdo, M. Dufour, S. Ithurria, H. Aubin, A. Ouerghi, E. Lacaze, M. G. Silly, B. Dubertret, and E. Lhuillier. Electronic structure of CdSe-ZnS 2D nanoplatelets *Appl. Phys. Lett* **2017**, 152103

(14) S. Shendre, S. Delikanli, M. Li, D. Dede, Z. Pan, S. Tung Ha, Y. Hsing Fu, P. L. Hernández-Martínez, J. Yu, O. Erdem, A. I. Kuznetsov, C. Dang, T. Chien Sum and H. Volkan Demir. Ultrahigh-efficiency aqueous flat nanocrystals of CdSe/CdS@$Cd_{1-x}Zn_xS$ colloidal core/crown@alloyed-shell quantum wells *Nanoscale* **2019**, *11*, 301-310

(15) Y. Altintas, U. Quliyeva, K. Gungor, O. Erdem, Y. Kelestemur, E. Mutlugun, M. V. Kovalenko, H. Volkan Demir. Highly Stable, Near-Unity Efficiency Atomically Flat Semiconductor Nanocrystals of CdSe/ZnS Hetero-Nanoplatelets Enabled by ZnS-Shell Hot-Injection Growth. *Small* **2019**, *15*, 1804854

(16) C. Meerbach, R. Tietze, S. Voigt, V. Sayevich, V. M. Dzhagan, S. C. Erwin, Z. Dang, O. Selyshchev, K. Schneider, D. R. T. Zahn, V. Lesnyak, A. Eychmüller. Brightly Luminescent Core/Shell Nanoplatelets with Continuously Tunable Optical Properties. *Adv. Optical Mater.* **2019**, *7*, 1801478

(17) A. W. Achtstein, O. Marquardt, R. Scott, M. Ibrahim, T. Riedl, A. V. Prudnikau, A. Antanovich, N. Owschimikow, J. K. N. Lindner, M. Artemyev and U. Woggon. Impact of Shell Growth on Recombination Dynamics and Exciton–Phonon Interaction in CdSe–CdS Core–Shell Nanoplatelets. *ACS Nano* **2018**, *12*, 9476-9483

(18) S. Luo, M. Kazes, H. Lin and D. Oron. Strain-Induced Type II Band Alignment Control in CdSe Nanoplatelet/ZnS-Sensitized Solar Cells. *J. Phys. Chem. C* **2017**, *121*, 11136-11143

(19) A. M. Smith, A. M. Mohs and S. Nie. Tuning the optical and electronic properties of colloidal nanocrystals by lattice strain. *Nature Nanotechnology* **2009**, *4*, 56–63

(20) S. Christodoulou, F. Rajadell, A. Casu, G. Vaccaro,J. Q. Grim, A. Genovese , L. Manna,J. I. Climente, F. Meinardi, G. Rainò, T. Stöferle, R. F. Mahrt, J. Planelles, S. Brovelli, I. Moreels. Band structure engineering via piezoelectric fields in strained anisotropic CdSe/CdS nanocrystals. *Nat Commun.* **2015**, *6*, 7905

(21) C. Segarra, J. I. Climente, A. Polovitsyn, F. Rajadell, I. Moreels and J. Planelles. Piezoelectric Control of the Exciton Wave Function in Colloidal CdSe/CdS Nanocrystals. *J. Phys. Chem. Lett.* **2016**, *7*, 2182-2188

(22) John P. Loehr Physics of Strained Quantum Well Lasers. *Springer US* **1998**

(23) A. Antanovich, A. W. Acthstein, A. Matsukovich, A. Prudnikau, P. Bhaskar, V. Gurin, M. Molinari and M. Artemyev. A strain-induced exciton transition energy shift in CdSe nanoplatelets: the impact of an organic ligand shell. *Nanoscale* **2017**, *9*, 18042-18053

(24) S. Christodoulou, J. I. Climente, J. Planelles, R. Brescia, M. Prato, B. Martin-Garcia, A. Hossain Khan and I. Moreels, Chloride-Induced Thickness Control in CdSe Nanoplatelets. *Nano Letters* **2018**, *18*, 6248-6254.

(25) M. Dufour, J. Qu, C. Greboval, C. Méthivier, E. Lhuillier, S. Ithurria. Halide Ligands To Release Strain in Cadmium Chalcogenide Nanoplatelets and Achieve High Brightness. *ACS Nano.* **2019**, *13*, 5326-5334

(26) F. Rajadell, J. I. Climente, and J. Planelles. Excitons in core-only, core-shell and core-crown CdSe nanoplatelets: Interplay between in-plane electron-hole correlation, spatial confinement, and dielectric confinement. *Phys. Rev. B* **2017**, *96*, 035307

(27) M. Richter. Nanoplatelets as material system between strong confinement and weak confinement. *Phys. Rev. Materials* **2017**, *1*, 016001

(28) M. Tadić, F. M. Peeters, K. L. Janssens, M. Korkusiński and P. Hawrylak. Strain and band edges in single and coupled cylindrical InAs/GaAs and InP/InGaP self-assembled quantum dots. *J. Appl. Phys.* **2002**, *92*, 5819

(29) F. Rajadell, M. Royo, and J. Planelles. Strain in free standing CdSe/CdS core-shell nanorods. *J. Appl. Phys.* **2012**, *111*, 014303

(30) G. H. V. Bertrand, A. Polovitsyn, S. Christodoulou, A. H. Khan and I. Moreels. Shape control of zincblende CdSe nanoplatelets. *Chem. Commun.* **2016**, *52*, 11975

(31) For light holes, the sign of the deformation potential is opposite to that of heavy holes. Therefore, core/shell strain splits heavy and light holes energetically in all the structures we study.

(32) B. M. Saidzhonov, V. F. Kozlovsky, V. B.Zaytsev, R. B. Vasiliev. Ultrathin CdSe/CdS and CdSe/ZnS core-shell nanoplatelets: The impact of the shell material on the structure and optical properties. *Journal of Luminescence* **2019**, *209*, 170-178.

(33) A. Szemjonov, T. Pauporté, S. Ithurria, B. Dubertret, I. Ciofini and F. Labat. Combined Computational and Experimental Study of CdSeS/ZnS Nanoplatelets: Structural, Vibrational, and Electronic Aspects of Core–Shell Interface Formation. *Langmuir* **2018**, *34*, 13828-13836

Graphical TOC Entry